Marine Biology 107, 83–91 (1990)

Marine Biology
International Journal on Life in Oceans and Coastal Waters

Mechanics and energetics of swimming in the small copepod *Acanthocyclops robustus* (Cyclopoida)*

M. J. Morris [1], K. Kohlhage [2] and G. Gust [3]

[1] Ocean Optics, Inc., Dunedin, Florida 34698, USA
[2] Universität Münster, Zoologisches Institut, D-4400 Münster, FRG
[3] University of South Florida, Department of Marine Science, St. Petersburg, Florida 33701-5016, USA

Date of final manuscript acceptance: May 18, 1990. Communicated by J.M. Lawrence, Tampa

Abstract. High-speed films of swimming *Acanthocyclops robustus* were used to test a crustacean swimming-model based on numerical analysis of thrust production. Predicted body velocities and jump distances were usually within 75% of those observed. Most of the thrust which propels. *A. robustus* is produced by movements of the 2nd, 3rd, and 4th thoracic swimming legs, with only small contributions from the first thoracic swimming legs. A model analyzed without the first antennae suggested that the antennae do not produce significant thrust. The leg and antennal movements could be described with trigonometric equations (cosine curves), but were best described by polynomial fits of position vs time data from the films. Patterns of swimming velocity varied among four episodes that were modeled, and followed differences in swimming-leg motions. Model results for the small (cephalothorax length = 0.6 mm) cyclopoid *A. robustus* and those which have been reported for the large calanoid copepod *Pleuromamma xiphias* and other swimmers indicate that mechanical efficiency (30%) does not scale with body size, whereas jump distance (one body length), proportion of thrust generated by hydrodynamic added mass (70%), and net cost of transport, C_p (40 to 109 cal g^{-1} km^{-1}) do.

Introduction

Direct measurement of the metabolic power used by small crustaceans to swim is restricted by the lack of suitably sensitive methods, but can be estimated from calculations of the mechanical power dissipated as drag. Results for copepods based on an assumed constant swimming-velocity suggest energy costs of locomotion that are negligible compared to standard metabolism (Vlymen 1970, Svetlichnyi et al. 1977). In contrast, analyses using the observed unsteady velocity-patterns of swimming copepods indicate costs that are an order of magnitude higher (Minkina and Pavlova 1981, Petipa 1981, Petipa and Ostravskaya 1984).

Numercial integration of the Morrison equation (Morrison et al. 1950) was used by Morris et al. (1985) to analyze the swimming energetics of a large calanoid copepod, *Pleuromamma xiphias* (cephalothorax length, ctl = 6 mm) by modeling the propulsion generated from known movements of its swimming appendages. In addition to quantifying the power required to move the appendages, the model of Morris et al. also provided a testable prediction of the temporal pattern of the copepod's swimming velocity. Results from that analysis substantiated the findings of Minkina and Pavlova (1981) and Petipa and Ostravaskaya (1984), i.e., the metabolic power used to swim was three to five times higher for *P. xiphias* than its standard metabolic rate. However, the analysis was based on the assumption that the temporal pattern of leg velocities was sinusoidal, the amplitudes and frequencies of the leg movements were extrapolated from data for different species, and the motions of the first antennae were not included in the calculation of thrust. The model predictions could not be confirmed, as actual temporal patterns of swimming velocities of *P. xiphias* were not available.

Here we report a test of the numerical model with the small copepod *Acanthocyclops robustus* (ctl = 0.6 mm). Our objectives were to: (1) compare observed and model-predicted swimming velocities, (2) determine the suitability of sinusoidal curves for describing swimming-leg motion, (3) examine the role of the first antennae in the propulsive process, (4) calculate possible wall-effects on confined individuals, and (5) compare the mechanics and energetics of swimming of the small cyclopoid copepod *A. robustus* to those of the larger calanoid copepod *Pleuromamma xiphias*.

Materials and methods

The model input parameters were determined from examination of high-speed (2 000 frames s^{-1}) films of *Acanthocyclops robustus*

* Please address all correspondence and requests for reprints to G. Gust at the University of South Florida, St. Petersburg

Table 1. *Acanthocyclops robustus*. Model parameters for four swimming episodes. Mass, length and cross-section were measured on 0.60 mm cephalothorax-length (ctl) specimens. Dimensions for smaller individuals were calculated by assuming constant shape

	Episode:			
	9-3	9-4	9-5	12-4
Temperature (°C)	22	22	22	12
ctl (mm)	0.60	0.60	0.45	0.55
Vol ($m^3 \times 10^{-12}$)	16.70	16.70	7.50	12.90
Mass ($kg \times 10^{-8}$)	1.71	1.71	0.77	1.32
Area ($m^2 \times 10^{-8}$)	4.37	4.37	2.46	3.67

swimming in a $10 \times 10 \times 1$ mm cuvette (Kohlhage 1983) together with measurements of the dimensions of preserved specimens. *A. robustus* swims in ≈ 1 body-length hops (episodes) which consist of the metachronal power strokes of the swimming legs and first antennae followed by return of the antennae and the collective packet of legs to their initial positions (see Kohlhage 1983 for detailed description). Episodes were selected in which the swimming trajectory was a straight path parallel to the focal plane of the camera, and the copepod was in lateral view and did not collide with other individuals during its leap. Wall effects resulting from the small size of the cuvette were modeled for one of the episodes. For a rigorous test of the model, the observed body-velocity patterns and jump distances need to vary significantly among episodes yet be correctly predicted by the model from changes in the input parameters alone. Four episodes were selected which met the above criteria in that leg and body-velocity patterns were distinctly different and both individual size and ambient temperature varied (Table 1).

Geometric dimensions

Body dimensions of preserved *Acanthocyclops robustus* (ctl = 0.6 mm) were measured under a dissecting microscope. Body cross-sections and volumes were calculated from the maximum and minimum diameters by assuming an elliptical shape. Body masses were calculated from these volumes and a density of 1.022 g cm^{-3} (Williams 1900).

Cross-sectional areas of the swimming legs during the power stroke and of the collective recovery-stroke packet were taken from the analysis by Kohlhage (1983, his Fig. 35) of an individual (ctl = 0.60 mm) swimming away from the camera (Fig. 1). It was assumed that water did not flow between the setae and setules during strokes, i.e., the legs acted as solid paddles. Flow of water through setae would tend to reduce the thrust produced by drag on the swimming legs, and calculations of flows through setae (Koehl et al. 1984) could be accommodated in our model if necessary.

The dimensions of the first antennae of a 0.50 mm-ctl individual are from Fig. 33 of Kohlhage (1983).

The body, swimming leg, and antennae dimensions of the three different-sized individuals that were modeled in the four episodes (ctl = 0.45, 0.55, 0.60, and 0.60 mm) were scaled to body length by assuming constant shape. A schematic drawing of a 0.6 mm ctl individual is shown in Fig. 1.

Movements of appendages

The swimming legs move as rigid paddles. Their motions were evaluated in each of the episodes from measurements of the angles (β) between the legs and the long axis of the body in successive (every 0.5 ms) frames of film, i.e., as a function of time (t).

Films of an individual viewed dorsally were used to investigate the pattern of antennae movements. While moving, the antennae

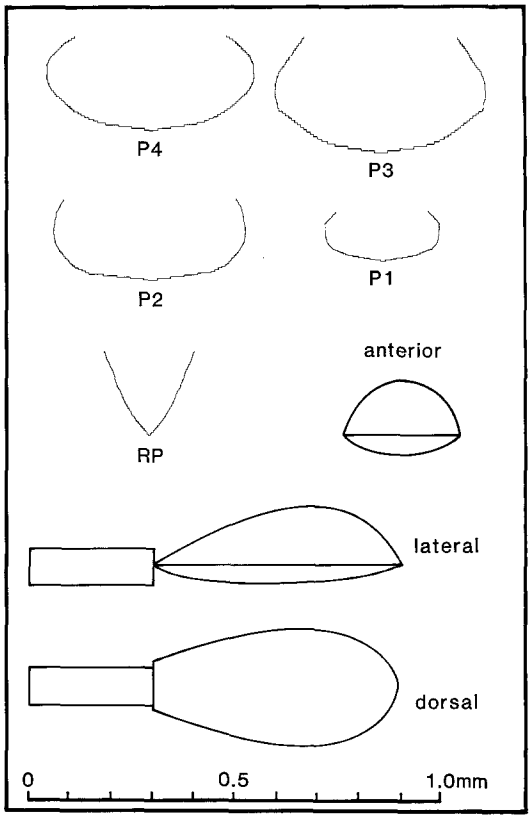

Fig. 1. *Acanthocyclops robustus*. Idealized drawing (cephalothorax length = 0.6 mm). Body area, volume, and mass were calculated from summation of thin sections through cephalothorax by assuming elliptical dorsal and ventral outlines; urosome was assumed to be cylinder; swimming legs (P1–P4) and recovery packet (RP) were flat paddles composed of 50 rectangular sections of uniform height but variable width. Although widths at attachment points are in some cases wider than model body, this discrepancy has little effect on model results because no thrust is generated in these regions of the legs

consisted of rigid basal and distal sections, each of which followed their own trajectories. The temporal pattern of antennal motions in the four laterally-viewed swimming episodes was assumed to vary only in duration (the antennae-stroke periods for these were reported by Kohlhage 1983).

Swimming-leg data were fit by least-squares to third-order polynomials. It was necessary to extend the stroke period of the legs by as much as 2 ms so that the derivative of the polynomial (equal to the angular velocity, ω) started and ended at zero. The data for antennal movements was not sufficiently precise to reveal accelerative phases of movement; consequently the data was fit to linear functions (constant ω). Both swimming-leg and antennae motions were also fit to cosine curves by measuring stroke period and amplitude between the observed starting and stopping times and positions. The cosine curves had the advantage of accurate stroke durations, and beginning and ending velocities of zero, but were based on only two data points. In contrast, the polynomials used all observed leg positions, but required extension of leg-stroke durations to include all phases of acceleration.

Mathematical modeling

The model, as outlined in detail in Morris et al. (1985), uses the equation of Morrison et al. (1950) to evaluate the in-line hydrodynamic force (F) acting on the copepod's body and/or on its moving

appendages:

$$F = M(dU/dt) + \varrho K_I \hat{V}(dU/dt) + 0.5\,\varrho C_d A U^2, \quad (1)$$

where M = the mass of the moving object (copepod body or a section of an appendage), K_I = the hydrodynamic added-mass coefficient, $\hat{V}$ = a characteristic volume of the object, C_d = the object's drag coefficient, A = the projected area normal to the direction of flow, U = velocity of the object relative to the fluid, ϱ = water density, and t = time. For this study, the model was modified by including the hinged first antennae in calculation of the thrust, and by introducing an iterative procedure to reduce the error inherent in numerical integration of second-order differential equations which contain a first derivative (Eisberg and Lerner 1981). Essentially, the thrust generated by a small segment of swimming leg is calculated during a finite time interval Δt from the velocity (U_n) and the acceleration ($\Delta U_n/\Delta t$) of the relative flow normal to the leg, where U_n (see Eq. 2 below) is a function of body velocity (V), ω, and β of the leg (Step 1). The local thrusts are summed over the lengths of all swimming legs that move during the particular time interval, thus yielding the total propulsive thrust (t). This total thrust (t) minus the body drag (D) is used to calculate the acceleration of the copepod body and its hydrodynamic added-mass during the specific interval (Step 2). The body velocity (V) resulting from the acceleration for the time interval is then calculated (Step 3). Repetition of the process results in the temporal pattern of body velocities.

Each of the equations in Steps 1–3 involves the body velocity V and, for each time interval, these equations must be either solved simultaneously or approximated. In Morris et al. (1985), the body velocity V was approximated in Steps 1 and 2 by using the value of V calculated for the endpoint of the previous time interval. In the present study, the analysis was refined by using the V calculated for the end of the previous interval as a first guess, solving for acceleration, revising the estimate of V at the midpoint of the new interval, and re-estimating acceleration. The iteration was repeated until two successive estimates of V were within 1% of each other.

Drag coefficients for the leg and antennae sections are calculated from the formula for a cylinder normal to flow (White 1974). The added mass of each leg segment is assumed as the mass of fluid contained in the cylinder generated by rotating the section about its axis (Blake 1979). The drag coefficient of the copepod body is taken from Vlymen (1970), and its added mass is calculated from the theoretical flow around a prolate spheroid as used by Vlymen (1970).

The first antennae of *Acanthocyclops robustus* were considered to consist of two rigid segments – a proximal segment of length $|AC|$ and a distal segment containing Point D (Fig. 2). The fluid flow past the proximal segment is calculated in a manner similar to that employed for the swimming legs. Measurements of the angle (β) between the proximal segment and the long axis of the body were fitted to functions of time. The derivative of this function is the angular velocity (ω). Relative flow normal to a position, B, on this segment (with positive values pointing in the direction of swimming, Fig. 2) is:

$$U_n = \omega\,|AB| - V \sin(\beta). \quad (2)$$

Measurements of the angle α between the distal segment and the long axis of the body were also fitted to functions of time. The position of a Point D on the distal segment is given by the sum of the position vectors $\overrightarrow{AB} + \overrightarrow{CD}$ (marked as Points A, C, D in Fig. 2). The time-derivative of the resultant vector, $\overrightarrow{AD}$, gives the velocity of Point D. The relative velocity of the flow (U_r) is $-|\overrightarrow{AD} + \vec{V}|$. The flow normal to the antennae segments (U_n) is equal to $U_r - U_1$ where U_1 is the vector projection of U_r on the position vector $\overrightarrow{CD}$.

The close proximity of walls in the confined cuvette could affect the swimming of the copepod, because the motion of the body would be slowed by the shear stress on the cuvette wall. The moving appendages would also react with the wall, except that this shear stress would increase the propulsive thrust and tend to speed-up the copepod's swimming. To estimate the magnitude of these wall effects, the local shear stress (τ) acting on a leg element, antennal segment or body segment was calculated from:

$$\tau = \varrho\, dU/dz, \quad (3)$$

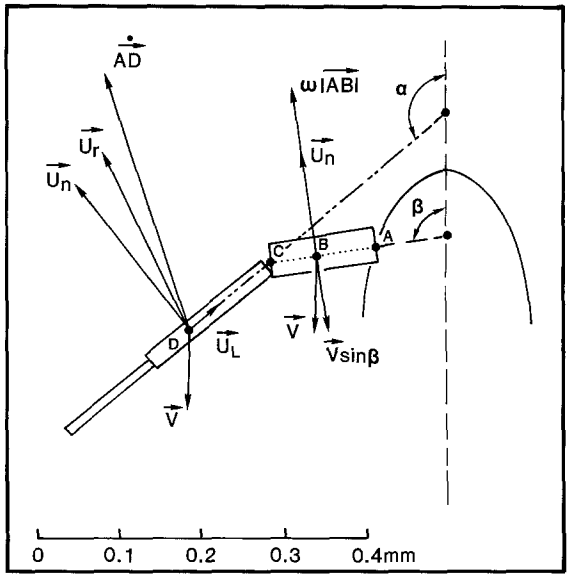

Fig. 2. *Acanthocyclops robustus.* Left first-antennae of a 0.5 mm cephalothorax-length copepod. The proximal segment (Point A to Point C) rotates through the angle β, while points on the distal segments move through angle α relative to the copepod's body. The flow of water past each segment (u_r) results from rotation of the segments ($\omega|\overrightarrow{AB}|$ for proximal and $\overrightarrow{AD}$ distal) and motion of the entire copepod ($\vec{V}$). The component of u_r normal to the segment is u_n, while the lateral component is u_L

where dU is the change in fluid velocity from its value near the copepod (equal to velocity of the particular leg, antennae or body segment) to zero at the cuvette wall; dz is the distance from the body part to the wall.

The force from the shear stress which contributes to the thrust of the appendages or drag of the body is:

$$F = \tau A, \quad (4)$$

where A is the effective area of the particular segment. The effective area of the leg segments for the copepod in Episode 9-3 was based on the area of the entrained water that moves with the leg (its hydrodynamic added mass) equal to the area of the circle generated by rotating the leg segment about its long axis. Because the shear stress acting on a particular element of entrained water is shielded by the entrained water of leg segments that are more distal to it, the effective area was calculated as the difference between the area of each leg segment's entrained water and that of its distal neighbor. Zero or negative areas meant that the segment was totally shielded. Thus, the water entrained by each leg segment was envisioned as a disc that moved parallel to the cuvette wall during each small time interval (Δt). The total wall effect on the legs was the sum of the effects on each segment and was added to the thrust for each Δt.

The effective area of antennae segments was calculated as the diameter of the antennae plus entrained water times segment length. In this case, both walls of the cuvette exerted shear stress, and the resulting force acted in the same direction as the motion of each antennal segment.

The effective area of the copepod body was determined by dividing the body into five sections. The urosome was assumed to be a cylinder whose projecting area was affected by two walls. The cephalothorax consisted of four sections that interacted only with the wall dorsal to the copepod (the ventral side was shielded by legs). The average projecting area of each section was equivalent to half of the maximum projecting area. The average height of each section was used to calculate dz. The copepod was assumed to be centered in the 1 mm-wide cuvette.

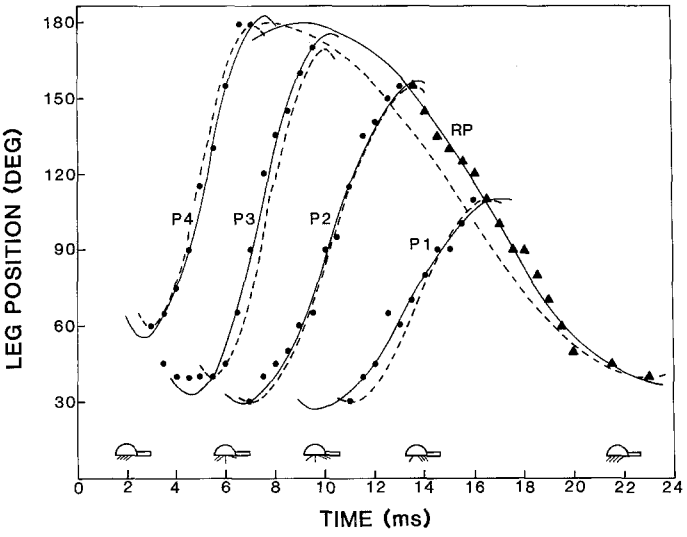

Fig. 3. *Acanthocyclops robustus.* Positions of swimming legs (P1–P4) vs time in Swimming Episode 9–4. Continuous curves are third-order polynomial fits to data; dashed curves are cosine curves, with amplitude and period calculated from observed starting and stopping points of leg rotation. Leg positions at various times are shown by sketches at bottom of figure

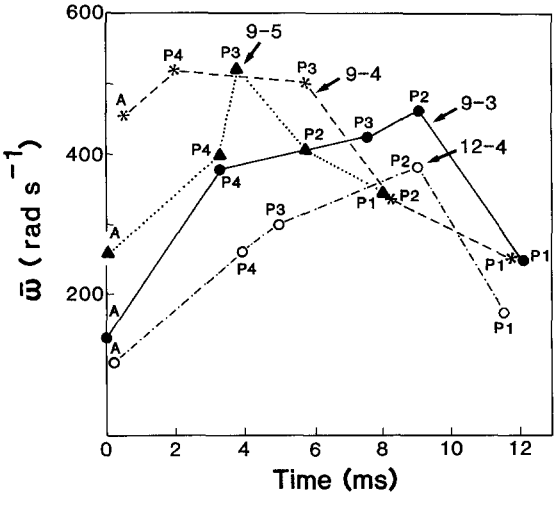

Fig. 4. *Acanthocyclops robustus.* Mean angular velocities (ω) and timing patterns of leg (P1–P4) and antennae (A) movements for four swimming episodes (9-3, 9-5, 9-6, 12-4). Data points represent mean angular velocity of legs or antennae and are plotted at midpoints of strokes. Lines connecting points are for graphical clarity only

Results

The time sequence of positions of the four swimming legs during Swimming Episode 9-4 shown in Fig. 3 is indicative of the general leg-motion patterns of *Acanthocyclops robustus*. The power stroke was initiated by an anterior to posterior rotation of the first antennae, followed by sequential (P4, P3, P2, P1) rotations of the thoracic swimming legs at mean angular velocities (ω) of 522, 504, 335, and 254 rad s^{-1}, respectively. In the recovery stroke, the legs returned as a collective packet at $\omega = -157$ rad s^{-1} to their initial positions simultaneously with the first antennae.

Table 2. *Acanthocyclops robustus.* Leg-movement parameters for Swimming Episode 9-4. Periods (t), amplitudes (A), and starting positions (β_0) were used in cosine equations to calculate positions and velocities of the four swimming legs (P1–4) and collective recovery packet (RP) in model analysis. Correlation coefficients (r^2) for positions predicted by cosine equation vs positions observed in the sequence of film frames are compared to correlation coefficients for positions predicted from polynomial equations fit by least-squares method

Swimming leg	Cosine function			Polynomial function	
	t (ms)	A (rad)	β_0 (rad)	r^2	r^2
P4	4.0	2.09	1.047	0.983	0.997
P3	4.5	2.27	0.698	0.990	0.998
P2	6.5	2.18	0.524	0.998	0.998
P1	5.5	1.40	0.524	0.988	0.997
RP	15.5	−2.44	3.142	0.972	0.996

Analysis of leg motions by fitting time (independent) and position (dependent) data to third-order polynomials resulted in higher correlation coefficients than did fitting the data to cosine curves (Table 2). However, the cosine-curve correlation coefficients were high (>0.97), which suggests that the accelerative and decelerative phases of the swimming-leg power strokes were of equal duration.

While the sequence of leg and antennae movements were similar in the four episodes analyzed, both ω and the timing of these movements varied. Episode 9-4 was characterized by rapid rotation of the antennae and P4 at the beginning of the power stroke, followed by rotations at decreasing ω of P3, P2, and P1 (Fig. 4). In contrast, ω of the copepod's swimming legs in Episode 9-3 increased steadily to a maximum value of 464 rad s^{-1} for P2, near the end of the power stroke. The leg-movement pattern in Episode 12-4, which was filmed in a low-temperature environment, was similar to those in Episode 9-3, but with reduced ω for all limbs. The power stroke of the smallest individual of Episode 9-5 was of shorter duration than that observed for all other episodes, and ω of the legs increased to a maximum of 522 rad s^{-1} for P3 midway through the power stroke, and then decreased for the remaining legs, P2 and P1.

The different patterns of leg movements resulted in different patterns of the copepod's body velocity (V_{obs}) that were observed. For example, V_{obs} reached its maximum value early in Episode 9-4 (at $t = 8$ ms) and relatively late in Episode 9-3 ($t = 12$ ms; Fig. 5). This matches the timing of maximum ω for these two episodes (5.75 and 9.00 ms, respectively; Fig. 4).

The body-velocity patterns predicted by the model were, in general, similar to those that were observed. Correlation coefficients measuring the similarity in temporal pattern (rather than magnitude) of body velocity predicted from polynomial fits for leg motion (V_p) vs V_{obs} ranged from 0.89 for Episode 9-4 to 0.62 for Episode 9-5. The similarity is evident in the early maximum of V_{obs} in Episode 9-4 and the late maximum in Episode 9-3, which are clearly predicted by the model (Fig. 5).

The magnitudes of V_p were either within measurement uncertainty (± 0.5 cm s^{-1}) of V_{obs} (especially dur-

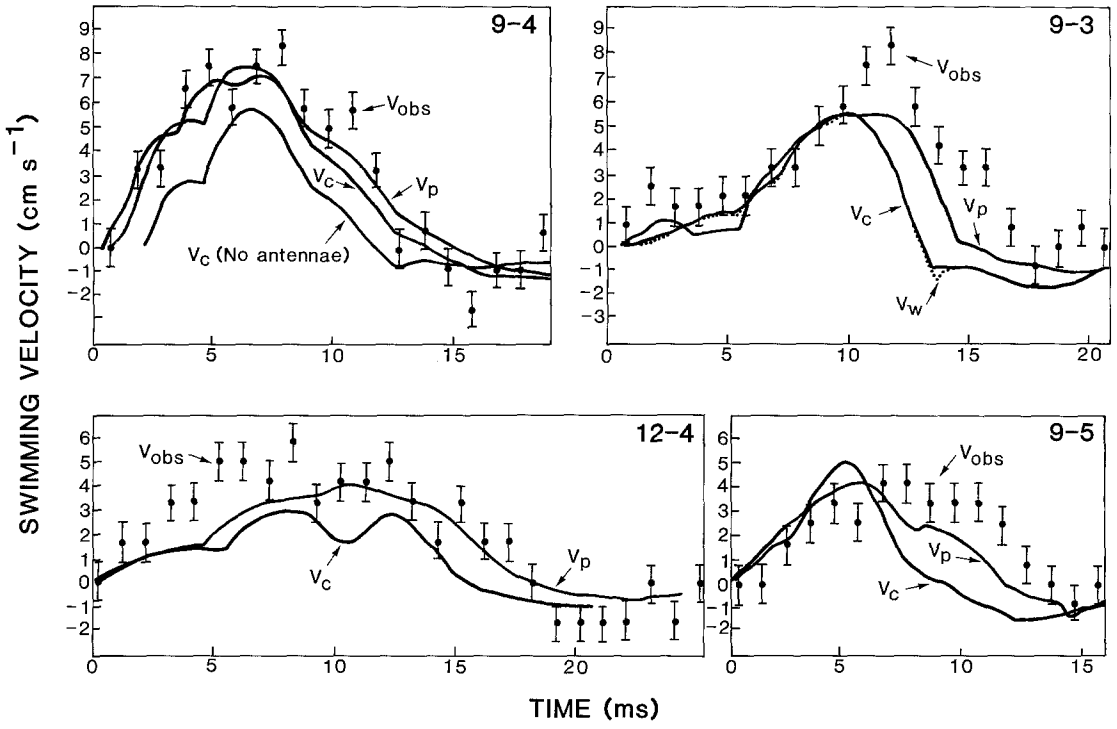

Fig. 5. *Acanthocyclops robustus.* Temporal patterns of observed body velocities (V_{obs}) and those predicted by model based on polynomial descriptions of leg movements (V_p), and on trigonometric functions for leg movements (V_c). V_w: predicted velocity with wall effects "turned on"

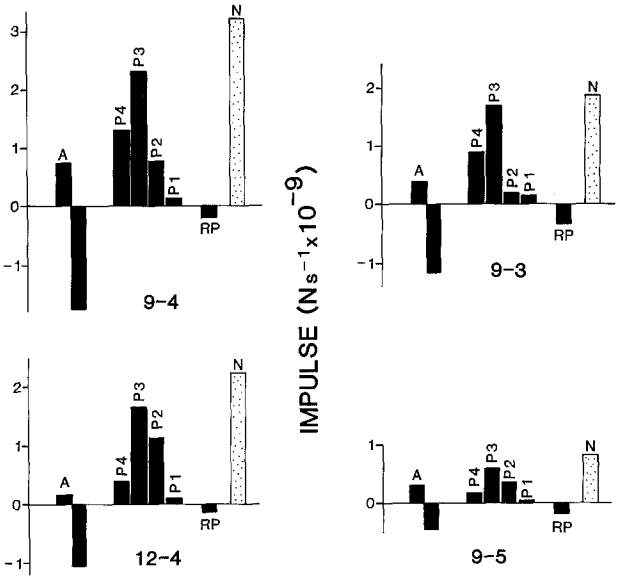

Fig. 6. *Acanthocyclops robustus.* Impulse produced by legs (P4–P1), recovery packet (RP), antennae (A), and net impulse (N) for four swimming episodes

ing the power stroke), or lower than the observed values (Fig. 5). Maximum values of V_p ranged from 65 to 100% of the observed maximum values (Table 3). Polynomial-based predictions of total distance travelled during the episodes were also lower than observed, ranging from 60 to 93% (Table 3).

The model predictions for maximum values of body velocity based on cosine-fitted curves for leg motions (V_c) were more accurate than the V_p for the three high-temperature episodes (9-3, 9-4, 9-5), but less accurate for Episode 12-4 (Table 3). However, cosine-based predictions for total jump distance were as low as 50% of observed jump distances (Table 3).

Model predictions of the impulse generated by each of the appendages for both power (+) and recovery (–) strokes for polynomial-based leg and antennae motions (Fig. 6) indicates that in all four episodes the antennae produced net negative impulse. Of the swimming legs, P3 produced the maximum impulse and P1 the minimum

Table 3. *Acanthocyclops robustus.* Comparison of velocities (V), jump distances (s) mechanical efficiencies (E), and net costs of transport (C) predicted by model based on polynomial descriptions of leg motions ($_p$) with model predictions based on trigonometric leg-motion functions ($_c$). Similarity of temporal patterns of V_p and observed velocities were tested with correlation analysis (Row 1, r^2 values). Maximum velocities and jump distances are ratios of predicted to observed

	Episode			
	9-3	94	9-5	12-4
V_p (r^2)	00.81	00.89	00.62	00.77
Max. V_p (ratio)	00.65	00.83	01.00	00.70
Max. V_c (ratio)	00.66	00.92	02.19	00.52
s_p (ratio)	00.60	00.93	00.72	00.78
s_c (ratio)	00.37	00.78	00.39	00.41
E_p (%)	30.20	30.50	15.00	34.90
E_c (%)	30.60	40.30	29.80	28.70
C_p (cal g^{-1} km^{-1})	61.90	63.10	108.70	40.00
C_c (cal g^{-1} km^{-1})	81.40	59.30	122.50	50.90

Table 4. *Acanthocyclops robustus*. Comparison of velocity (V), jump distance (s) and net cost of transport (C) predicted for Episode 9-3, with and without wall-effects, calculated for body, legs and antenna

	$V_{max.}$ (cm s^{-1})	s (mm)	C (cal g^{-1} km^{-1})
No wall effects	5.51	0.22	81.5
Leg wall-effects	5.64	0.24	74.4
Leg and antenna wall-effects	5.65	0.24	73.3
Leg, antenna and body wall-effects	5.48	0.22	80.1

impulse. The recovery stroke of the swimming legs produced relatively small negative impulse. Differences in patterns of leg movements are reflected in the relative contributions of P2 and P4 to the impulse balance among the episodes.

The mechanical efficiency predicted by the polynomial-based model was about 30% for three of the episodes but was considerably lower (15%) for the small individual of Jump 9-5 (Table 3). Costs of transport (C_p) were low for the three large individuals (40 to 62 cal g^{-1} km^{-1}) and high for the small copepod (109 cal g^{-1} km^{-1}).

Efficiencies and costs of transport based on the model with cosine approximations for the leg motions were slightly higher than the polynomial-based predictions. In Jump 9-3, the effects of the walls of the cuvette were modeled. The predicted velocities with wall effects "turned on" (V_w) were slightly lower than without wall effects (Fig. 5). Separate calculations with wall effects turned on or off for legs, antenna and body are shown in Table 4. The wall shear-stress increased the thrust produced by the legs, leading to a higher maximum velocity, jump distance and lower cost of transport. Wall shear-stress on the body decreased maximum velocity and jump distance and increased cost of transport. In all cases the effects were $<5\%$.

Discussion

There are few data in the literature with which to directly compare the model predictions. Alcaraz and Strickler (1988) measured the force exerted by an individual tethered to a spring for the larger copepod *Cyclops scutifer* (ctl = 1 mm). The maximum force reported for *C. scutifer*, 0.66 dyn, was seven to ten times larger than the maximum thrusts calculated in the present study for *Acanthocyclops robustus*. This may be due to the tethering of *C. scutifer*. If we assume that behavior (i.e., the oscillation period for the swimming legs) and muscle power are the same for both tethered and non-tethered crustaceans, then the work produced by each must be equal. The tethered individual exerts a force over a distance restricted by the tether (0.040 mm for *C. scutifer*), which is much shorter than a free-swimming individual moves (typically one body length). Consequently, the force exerted by the tethered crustacean will be larger. The mechanical work reported for the jump by *C. scutifer* (3.3×10^{-11} cal) was similar to the work calculated by the model for *A. robustus* (2.4×10^{-11} cal).

The accuracy of the swimming model is evident in the similarity of the temporal patterns of predicted and observed body velocities. The velocities predicted by the model were within the experimental uncertainty for half of the observed velocities, and the timing of maximum predicted velocity was either coincident with that observed, or displaced by <2 ms (Fig. 5). This indicates that the observed differences in velocity patterns were caused by variations in swimming-leg motions, and that the model is sensitive to these variations. This is especially evident from the comparison of Episodes 9-3 and 9-4, where all model parameters were identical except the timing and angular velocities of the swimming legs.

The accuracy of the model's predictions depends on the accuracy of the input parameters used and on the reliability of the assumptions made in the model formulation. An analysis of the effects of errors in input parameters on model predictions was made by changing a single input parameter to ± 5, 25, and 50% of its original value while keeping the other parameters constant. The newly calculated jump distance was then compared to its original value. Jump distance was chosen as it was the least accurate of the model predictions. The analysis indicated that jump distance was most sensitive to changes in swimming-leg dimensions, body drag, swimming-leg added-mass coefficient, swimming-leg movement parameters, and fluid properties (Fig. 7), and relatively insensitive to changes in body mass, leg-drag, and body added-mass coefficient. The differences between predicted and observed jump distances can be explained by experimental errors in these parameters at the percentage level where each input-parameter error curve intercepts the observed jump distance (horizontal dashed lines in Fig. 7). For example, a 25% error in leg dimensions alone would account for the jump distance error in three out of four episodes. When all the parameters (except viscosity and density) are changed (either raised or lowered so as to produce the maximum cumulative effect), only a 5% error level is required to account for the differences between model prediction and observed jump distance for the least satisfactory episode, 9-5. Although actual uncertainty intervals for input parameters were not evaluated, it is unlikely that their uncertainty was less than $\pm 10\%$ (fluid viscosity and density excepted). Therefore, the model appears to be accurate within the limits of reliability of the input parameters and it is not possible with the present experimental data-set to detect errors in the underlying model assumptions (see Morris et al. 1985 for a discussion of these).

The sensitivity of model predictions to changes in leg-motion parameters (Fig. 7) and the differences between results based on polynomial vs trigonometric descriptions of leg movements (Table 3) indicate that leg motions must be observed at high filming rates to achieve accurate model predictions. This is because leg acceleration provides most of the thrust, and must be calculated

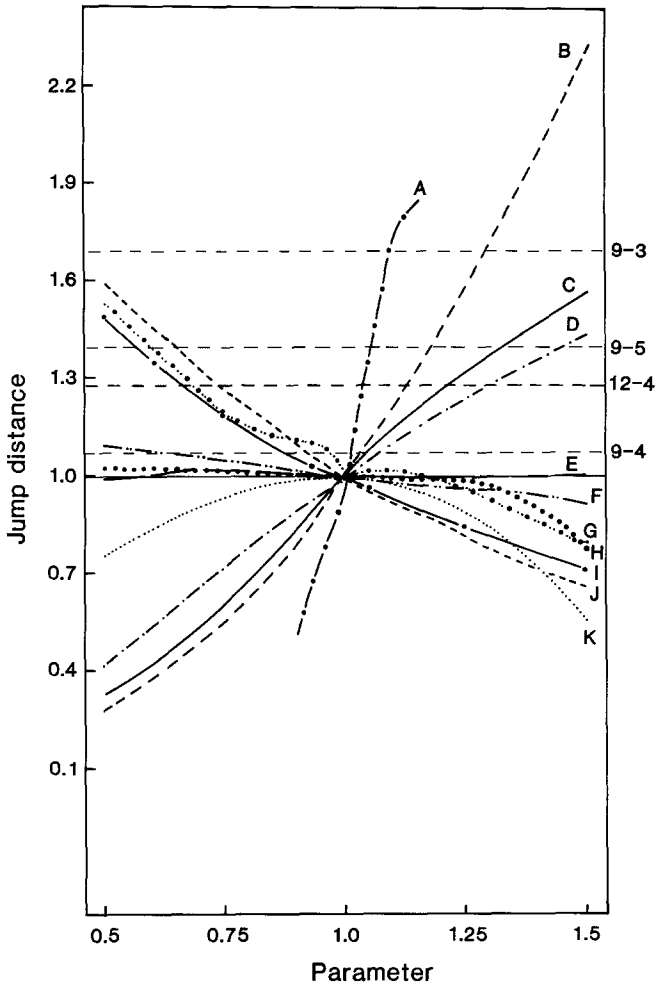

Fig. 7. *Acanthocyclops robustus*. Sensitivity of model-predicted jump distance to errors in model parameters. Jump distance is shown as ratio of predicted jump distance after parameter was adjusted by factor indicated by abscissa to original jump-distance prediction. Curve A indicates combined effects of changes in all parameters. Effects from changes in one parameter at a time are indicated by: B, swimming-leg dimensions; C, swimming-leg added-mass coefficient; D, fluid density; E, body mass; F, leg-drag; G, swimming-leg period; H, body added-mass coefficient; I, fluid viscosity; J, body drag; K, swimming-leg amplitude. Horizontal dashed lines represent observed jump distances for four swimming episodes (9-3, 9-4, 9-5, 12-4). Intersections of parameter error curves with jump-distance lines indicate error level necessary in a single parameter to account for difference between predicted and observed jump distances

from second derivatives of the observed time vs position data-pairs. Although not as accurate, the cosine description of leg motion appears to be suitable for situations where high filming rates are unavailable and/or the levels of accuracy indicated in Table 3 are acceptable.

The predictions for body velocity were low in Episodes 9-3 and 9-5 during the decelerative phase. Coincidentally, the model predicted large negative thrusts as the legs slowed to their posterior positions. Although the differences between predicted and observed velocities at this stage may be due to errors in model parameters, another explanation is suggested by the observation of lateral flexings of the swimming legs made by Kohlhage (1983). Thrust can only be generated by an accelerating limb (discounting contributions made by drag) if the sweep of the stroke is displaced towards the posterior of the copepod, and is maximized when the stroke of the appendage extends from $\beta = 60°$ to 180° relative to the body axis (Daniel 1984). The leg must decelerate the added mass of the fluid entrained by it at the end of its stroke, giving rise to negative thrust. The forward component of thrust, however, depends on the angle between leg and body (see Eq. 1). When positive thrust is generated, the leg is nearly perpendicular to the body and the thrust is pushing in line with the direction of travel. The leg decelerates and produces negative thrust as the leg-body angle approaches 180° and the thrust is becoming perpendicular to the line of travel. For Episodes 9-3 and 9-5 the model closely predicts positive thrust during the first half of the leg motions, but over-estimates negative thrust during the second half. It is possible that the legs of *Acanthocyclops robustus* shed some of their entrained water, i.e., reduce their added mass, by laterally squeezing the endopods and exopods together as the swimming legs decelerate at the end of the power stroke. This lateral contraction of the leg area was observed in several swimming episodes (Kohlhage 1983). It was not possible, however, to determine if contraction took place in the episodes modeled here due to the lateral perspective of the camera.

The model allows examination of various aspects of the locomotion process in copepods. For example, the impulse produced by the recovery movement of swimming legs was as low as 7% of the net propulsive impulse, and in all cases was less than the recovery impulse of the first antennae. This indicates that copepods have evolved an energy-efficient method of moving their legs back to their initial positions. They accomplish this by shielding the posterior legs from fluid resistance with the anterior legs, and by reducing the cross-section of the packet with lateral contraction of the endopods and exopods (see Fig. 1).

The net negative impulse provided by the antennae suggests that, although these organs are longer than the swimming legs, they are unimportant to the locomotion process. They may instead function as stabilizers or as supports for sensory organs (Strickler and Bal 1973). To test this hypothesis, the antennae in Episode 9-4 were "turned off" (i.e., without antennae) and the model run again. The resulting body-velocity pattern (Fig. 5) was similar to the analysis with antennae, except that the magnitudes of the velocities were all lower, the jump distance decreased by 16%, and maximum V_c decreased by 18%. Mechanical efficiency increased to 40%, while cost of transport was slightly lower. These results indicate that the antennae may be important in achieving maximum velocity and jump distance during an escape response, but may be energetically expensive for long-range swimming movements such as vertical migrations.

A comparison of the model results for the *Acanthocyclops robustus* with *Pleuromamma xiphias* suggests that mechanical efficiency does not scale with body size. Both copepods had efficiencies of about 30%, which is similar to the values calculated for much larger paddlers (Blake

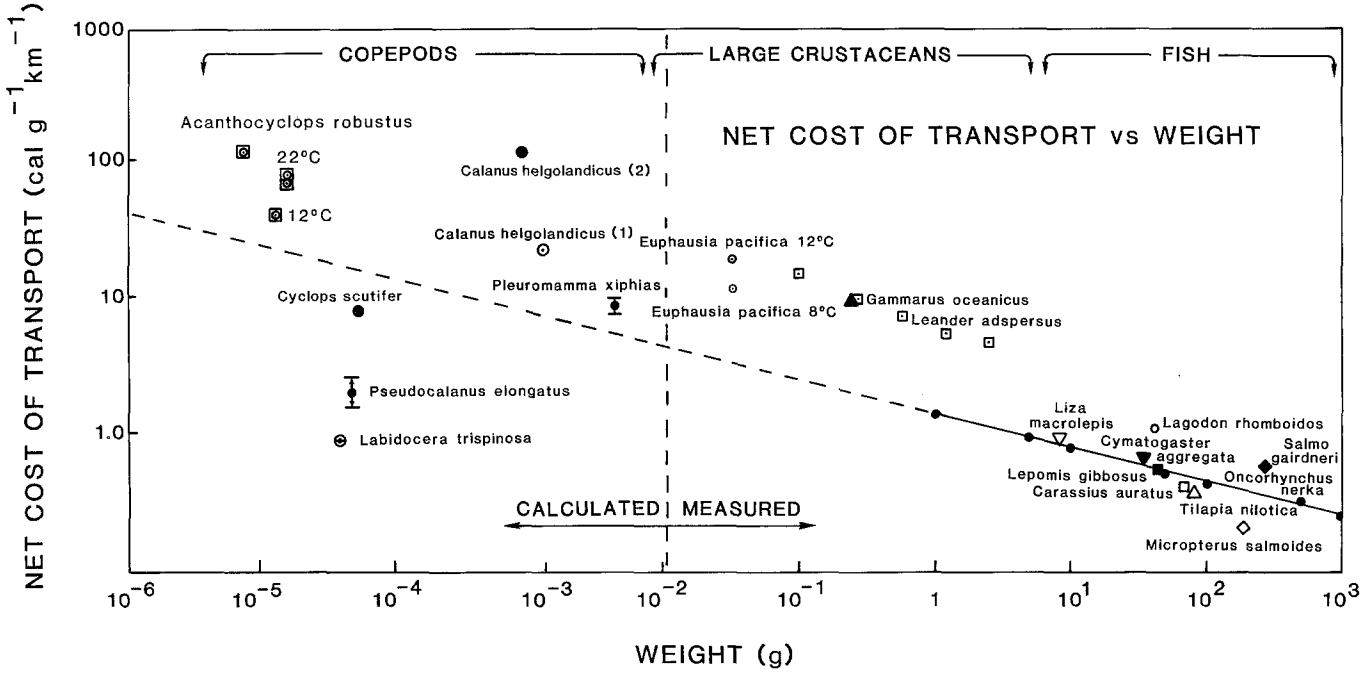

Fig. 8. *Acanthocyclops robustus*. Net cost of transport as a function of body weight for various swimming animals (after Schmidt-Nielson 1972 and Beamish 1978). Measured values were determined from oxygen consumed at 75% of critical swimming speed when data were available; when not, averaged swimming speed was used; temperatures for measured values were 15 °C or that closest to 15 °C; continuous portion of regression line represents net cost of transport (y; cal g^{-1} km^{-1}) vs weight (w; g) for *Oncorhynches nerka* ($y = 1.416\ w^{-0.25}$) between 1 and 1 000 g, from data in Brett and Glass (1973); dashed portion is extrapolation of this into weight values typical of zooplankton species, for purposes of comparison; data for measured values are for *Carassiius auratus*, Smit et al. 1971; *Cymatogaster aggregata*, Webb 1975; *Euphausia pacifica*, Torres and Childress 1983; *Gammarus oceanicus*, Halcrow and Boyd 1967; *Lagodon rhomboides*, Wohlschlag et al. 1968; *Lepomis gibbosus*, Brett and Sutherland 1965; *Liza macrolepis*, Kutty 1969; *Micropterus salmoides*, Beamish 1970; *Salmo gairdneri*, Webb 1971; *Tilapia nilotica*, Farmer and Beamish 1969; and *Leander adspersus*, Ivlev 1963. Calculated values are based on steady swimming-velocity (*Labidocera trispinosa*, Vlymen 1970; *Pseudocalanus elongatus*, Svetlichnyi et al. 1977); force measurements (*Cyclops scutifer*, Alcarez and Strickler 1988); or unsteady swimming-velocity (*Acanthocyclops robustus*, present study; *Pleuromamma xiphias*, Morris et al. 1985; *Calanus helgolandicus* (1), Minkina and Pavlova 1981; *C. helgolandicus* (2), Svetlichnyi 1987)

1980). However, *A. robustus* has zero or negative velocities at the end of its recovery stroke and moves on the average about one body length per episode, whereas larger copepods have coasting stages (Petipa 1981, Morris et al. 1985) and may move several body lengths per episode.

The importance of hydrodynamic added-mass to thrust production did vary with size. In *Pleuromamma xiphias,* roughly 30% of the thrust was produced by accelerating the water entrained by the legs compared to 75% for *Acanthocyclops robustus*. This may be related to the relative sizes of the legs. The length of P4 of *P. xiphias* is approximately 25% of the ctl, while the length of P4 in *A. robustus* is nearly 43% of ctl. The tips of the swimming legs of *A. robustus* remain almost stationary during the one-body-length swimming hop. The process might better be described as "walking" rather than "paddling" through the water.

The model's accuracy is also indicated by the comparison of predicted net cost of transport with those reported for other swimming animals (Fig. 8). The model predictions indicate that cost of transport for crustaceans scales to body mass with a slope that is similar to that of fish (dashed line in Fig. 8), but with a higher intercept. The model predictions for the small copepod *Acanthocyclops robustus* and the larger copepod *Pleuromamma xiphias* (Morris et al. 1985) agree with both the theoretical calculations for the copepod *Calanus helgolandicus* [Minkina and Pavlova 1981; *C. helgolandicus* (1) in present Fig. 8] and directly measured values for shrimps, euphausiids, and decapods. Costs of transport have also been calculated from the measured forces exerted by tethered *C. helgolandicus* [Svetlichnyi 1987; *C. helgolandicus* (2) in present Fig. 8] and *Cyclops scutifer* (Alcaraz and Strickler 1988). The value for *Calanus helgolandicus* is higher than would be expected from the other crustacean data, possibly because they were measured during a "flight reaction" stimulated by electric shocks. During escape movements, it is reasonable to assume that acceleration and speed are important and metabolic cost unimportant to *C. helgolandicus*. The value for *Cyclops scutifer,* in contrast, is lower than expected. The reasons for this are unclear, but may be due to the effects of tethering on the forces exerted by the swimming legs. Because the individual used by Alcaraz and Strickler was glued to a circular spring, the measured force may not be equivalent to thrust in an untethered specimen. Also, a jump distance of one body length was arbitrarily assumed in our calculation as actual data were not presented.

The temperature-dependence of cost of transport as predicted by the model for *Acanthocyclops robustus* has been observed for the euphausiid *Euphausia pacifica*

(Torres 1984). This temperature-dependence might be due to changes in density and viscosity of the water. However, when these parameters were changed from 12° values to 22° levels for Episode 12-4, and the model run again, cost of transport was not significantly changed. Kohlhage (1983) proposed that the lower cost of transport for *A. robustus* was a consequence of the lower power output of the copepod's muscles at low temperatures, and the resulting slower swimming speeds. This was tested by comparing the metabolic power predicted by the swimming model for the three high-temperature episodes with that of the low-temperature episode. The resulting Q_{10} value was 2.01, which is typical for poikilotherm muscle (Gordon 1977) and supports Kohlhage's hypothesis.

The model is successful at predicting observable swimming behavior to within 25% (swimming velocities and jump distances) and, by inference, the predicted energetic costs should be as accurate. Using the technique requires detailed analysis of both the dimensions and motions of the swimming appendages; however, it appears that sinusoidal patterns of appendage velocity may be adequate approximations to the actual motions. The model is applicable to a wide spectrum of body sizes and swimming appendages, and numerical experiments may be performed that are otherwise impossible (such as changing density and viscosity without changing temperature and migration simulations).

Acknowledgements. The authors would like to thank Ms. D. Walton for preparing the graphics. The first and third authors were supported by a grant from the Faculty Research and Creative Scholarship Fund of the University of South Florida.

Literature cited

Alcaraz, M., Strickler, J. R. (1988). Locomotion in copepods: pattern of movements and energetics of *Cyclops*. Hydrobiologia 167/168: 409–414

Beamish, F. W. H. (1970). Oxygen consumption of largemouth bass *Micropterus salmoides* in relation to swimming speed and temperature. Can. J. Zool. 48: 1221–1228

Beamish, F. W. H. (1978). Swimming capacity. In: Hoar, W. S., Randall, D. J. (eds.) Fish physiology. Vol. 7. Academic Press, London and New York, p. 101–187

Blake, R. W. (1979). The mechanics of labriform locomotion. I. Labriform locomotion in the angelfish (*Pterophyllum cimekei*): an analysis of the power stroke. J. exp. Biol. 82: 255–271

Blake, R. W. (1980). The mechanics of labriform motion. II. An analysis of the recovery stroke and the overall fin beat cycle propulsive efficiency in the angelfish. J. exp. Biol. 85: 337–342

Brett, J. R., Glass, N. R. (1973). Metabolic rates and critical swimming speeds of sockeye salmon (*Oncorhynchus nerka*) in relation to size and temperature. J. Fish Res. Bd Can. 30: 379–387

Brett, J. R., Sutherland, D. B. (1965). Respiratory metabolism of pumpkinseed (*Lepomis gibbosus*) in relation to swimming speed. J. Fish. Res. Bd Can. 22: 405–409

Daniel, T. L. (1984). Unsteady aspects of aquatic locomotion. Am. Zool. 24: 121–134

Eisberg, R. M., Lerner, L. S. (1981). Physics, foundations and applications. McGraw Hill, New York

Farmer, G. J., Beamish, F. W. H. (1969). Oxygen consumption of *Tilapia nilotica* in relation to swimming speed and salinity. J. Fish. Res. Bd Can. 26: 2807–2821

Gordon, N. S. (1977). Animal physiology: principles and adaptations. MacMillan, New York

Halcrow, K., Boyd, C. M. (1967). The oxygen consumption and swimming activity of the amphipod *Gammarus oceanicus* at different temperatures. Comp. Biochem. Physiol. 23: 233–242

Ivlev, V. S. (1963). Energy consumption during the motion of shrimps. Zool. Zh. 42: 1465–1471

Koehl, M. A. R., Cheer, A. Y. L., Paffenhöfer, G. A. (1984). Water flow around and particle capture by bristled appendages of zooplankton. EOS Trans., Am. geophys. Un. 60: p. 925

Kohlhage, K. (1983). Lokomotionsstudien an schwimmenden Copepoden. Diplomarbeit, Zoologisches Institut Universität Münster, Münster, FRG

Kutty, M. N. (1969). Oxygen consumption in the mullet *Liza macrolepsis* with special reference to swimming velocity. Mar. Biol. 4: 239–242

Minkina, N. I., Pavlova, E. V. (1981). Hydrodynamic drag and power at variable swimming in *Calanus helgolandicus* (Claus). Ehkol. Morei 7: 63–75

Morris, M. J., Gust, G., Torres, J. J. (1985). Propulsion efficiency and cost of transport for copepods: a hydromechanical model of crustacean swimming. Mar. Biol. 86: 283–295

Morrison, J. R., O'Brien, M. P., Johnson, J. W., Schaat, S. A. (1950). The forces exerted by surface waves on piles. J. Petrol. Technol. 189(TP2846): 149–189

Petipa, T. S. (1981).Trophic dynamics of copepods in marine planktonic systems. [In Russ.]. Naukowa Dumka, Kiev

Petipa, T. S., Ostravskaya, N. A. (1984). Assessment of active metabolism and efficiency of use of chemical energy by migrating copepods. Oceanology, Wash. 24: 631–636

Schmidt-Nielson, K. (1972). Locomotion: energy cost of swimming, flying, and running, Science, N.Y. 177: 222–228

Smit, H., Amelink-Koutstall, J. M., Vijverberg, J., von Vaupel-Klein, J. C. (1971). Oxygen consumption and efficiency of swimming goldfish. Comp. Biochem. Physiol. 39A: 1–28

Strickler, J. R., Bal, A. K. (1973). Setae on the first antennae of the copepod *Cyclops securifer* (Sars): their structure and importance. Proc. natn. Acad. Sci. U.S.A. 70: 2656–2659

Svetlichnyi, L. S. (1987). Speed, force and energy expenditure in the movement of copepods. Oceanology, Wash. 27: 497–502

Svetlichnyi, L. S., Zagorodnyaya, Y. A., Stepanov, V. N. (1977). Bioenergetics of copepods *Pseudocalanus elongatus* during migration. Soviet J. mar. Biol. 3: 430–436

Torres, J. J. (1984). Relationship of oxygen consumption to swimming speed in *Euphausia pacifica*. II. Drag, efficiency and a comparison with other swimming organisms. Mar. Biol. 78: 231–237

Torres, J. J., Childress, J. J. (1983). Relationship of oxygen consumption to swimming speed in *Euphausia pacifica*. I. Effects of temperature and pressure. Mar. Biol. 74: 79–86

Vlymen, W. J. (1970). Energy expenditure of swimming copepods. Limnol. Oceanogr. 15: 348–356

Webb, P. W. (1971). The swimming energetics of trout. (I). Oxygen consumption and swimming efficiency. J. exp. Biol. 55: 521–540

Webb, P. W. (1975). Efficiency of pectoral-fin propulsion of *Cymatogaster aggregata*. In: Wu, T. Y. T., Brokaw, C. J., Brennen, C. (eds.) Swimming and flying in nature. Plenum Press, New York, 573–584

White, F. M. (1974). Viscous fluid flow. McGraw-Hill, New York

Williams, S. R. (1900). The specific gravity of some freshwater animals in relation to their habits, development, and composition. Am. Nat. 34: 95–108

Wohlschlag, D. E., Cameron, J. N., Cech, J. J., Jr. (1968). Seasonal changes in the respiratory metabolism of the pinfish (*Lagodon rhomboides*). Contr. mar. Sci. Univ. Tex. 13: 89–104